Optimizing LIGO with LISA forewarnings to improve black-hole spectroscopy

Rhondale Tso,[1,*] Davide Gerosa,[1,2,†] and Yanbei Chen[1,‡]

[1]*TAPIR 350-17, California Institute of Technology, 1200 East California Boulevard, Pasadena, California 91125, USA*
[2]*School of Physics and Astronomy and Institute for Gravitational Wave Astronomy, University of Birmingham, Birmingham B15 2TT, United Kingdom*

The early inspiral of massive stellar-mass black-hole binaries merging in LIGO's sensitivity band will be detectable at low frequencies by the upcoming space mission LISA. LISA will predict, with years of forewarning, the time and frequency with which binaries will be observed by LIGO. We will, therefore, find ourselves in the position of knowing that a binary is about to merge, with the unprecedented opportunity to optimize ground-based operations to increase their scientific payoff. We apply this idea to detections of multiple ringdown modes, or black-hole spectroscopy. Narrow-band tunings can boost the detectors' sensitivity at frequencies corresponding to the first subdominant ringdown mode and largely improve our prospects to experimentally test the Kerr nature of astrophysical black holes. We define a new consistency parameter between the different modes, called δGR, and show that, in terms of this measure, optimized configurations have the potential to double the effectiveness of black-hole spectroscopy when compared to standard broadband setups.

I. INTRODUCTION

The first detection of merging black-hole (BH) binaries by the LIGO ground-based detectors is one of the greatest achievements in modern science. Some of the binary component masses are as large as $\sim 30\ M_\odot$ and unexpectedly exceed those of all previously known stellar-mass BHs [1]. These systems might also be visible by the future spaced-based detector LISA, which will soon observe the gravitational-wave (GW) sky in the mHz regime [2]. LISA will measure the early inspiral stages of BH binaries, predicting, with years to weeks of forewarning, the time at which the binary will enter the LIGO band [3]. This will allow electromagnetic observers to concentrate on the source's sky location, thus increasing the likelihood of observing counterparts. Multiband GW observations have the potential to shed light on BH formation channels [4–10], constrain dipole emission [11], enhance searches and parameter estimation [12,13], and provide new measurements of the cosmological parameters [14,15].

Here we explore the possibility of improving the science return of ground-based GW observations by combining LISA forewarnings to active interferometric techniques. LISA observations of stellar-mass BH binaries at low frequencies can be exploited to prepare detectors on the ground in their most favorable configurations for a targeted measurement. Optimizations can range from the most obvious ones (for instance, just ensuring the detectors are operational) to others that require more experimental work, like changing the input optical power, modifying mirror transmissivities and cavity tuning phases, and changing the squeeze factor and angle of the injected squeeze vacuum (see, e.g., Ref. [16]). Tuning the optical setup of the interferometer can allow us to boost the signal-to-noise ratio (SNR) of specific features of the signal "on demand" (only at the needed time, only at the needed frequency).

In particular, we apply this line of reasoning to the so-called *black-hole spectroscopy*: testing the nature of BHs through their ringdown modes. Narrow-band tunings were previously explored for studying the detectability of neutron-star mergers [17–19] and stochastic backgrounds [20], and are here proposed for BH science for the first time.

The perturbed BH resulting from a merger vibrates at very specific frequencies. These quasinormal modes of oscillation are damped by GW emission, resulting in the so-called BH ringdown [21,22]. If BHs are described by the Kerr solution of general relativity (GR) [23], all these resonant modes are allowed to depend on two quantities only: the mass and spin of the perturbed BH [24–26]. This is a consequence of the famous *no-hair theorems*: as two BHs merge, all additional complexities (hair) of the spacetime are dissipated away in GWs, and a Kerr BH is left behind. The detection of the frequency and decay time of one quasinormal mode can therefore be used to infer the mass and spin of the postmerger

*[*]rtso@caltech.edu
[†]dgerosa@caltech.edu
[‡]yanbei@caltech.edu

124043-1

FIG. 1. GW amplitude $\sqrt{S_h} = 2|\tilde{h}|/\sqrt{f}$ of a black-hole binary source similar to GW150914 compared to the noise curves $\sqrt{S_n}$ of LISA [37], LIGO [38], and a planned third-generation detector [39] (both in their broadband configurations and with narrow-band tunings). Optimized narrow banding enhances (decreases) the detector sensitivity around the frequency f_{33} (f_{22}) of the first subdominant (dominant) mode of the BH ringdown. The BH binary waveform is generated using the approximant of Ref. [40] with $m_1 + m_2 = 65\ M_\odot$, $q = 0.8$, $D = 410$ Mpc, $\iota = 150°$, assuming optimal orientation ($\theta = \phi = \psi = 0$).

BH. Measurements of each additional mode provide consistency tests of the theory. This is the main idea behind BH spectroscopy: much like atoms' spectral lines can be used to identify nuclear elements and test quantum mechanics, quasinormal modes can be used to probe the nature of BHs and test GR [27–30]. Despite its elegance, BH spectroscopy turns out to be challenging in practice, as it requires loud GW sources and improved data analysis techniques [31–36].

The main idea behind our study is illustrated in Fig. 1. A GW source like GW150914 emits GWs at ∼0.1 Hz and is visible by LISA with SNR ∼ 5. After ∼10 years, the emission frequency reaches ∼10 Hz and the source appears in the sensitivity band of LIGO or a future ground-based detector. The excitation amplitude of the dominant quasinormal mode is ∼10 times higher than the first subdominant mode. The latter is likely going to be too weak to perform BH spectroscopy. Optimized narrow-band tunings can boost the detectability of the weaker mode at the expense of the rest of the signal, making BH spectroscopy possible.

This paper is organized as follows: In Secs. II and III, we introduce BH spectroscopy and narrow-band tunings, respectively. Our results are illustrated in Sec. IV. We draw our conclusions in Sec. V. Hereafter, we use geometric units $c = G = 1$.

II. BLACK-HOLE SPECTROSCOPY

A. Black-hole ringdown

Let us consider a perturbed BH with detector-frame mass M and dimensionless spin j. GW emission during ringdown

can be described by a superposition of damped sinusoids, labeled by $l \geq 2$, $0 \leq |m| \leq l$, and $n \geq 0$ [41]. For simplicity, we only consider the fundamental overtone $n = 0$.

Each mode is described by its frequency ω_{lm} and decay time τ_{lm}. The GW strain can be written as [42,43]

$$h(t) = \sum_{l,m>0} B_{lm} e^{-t/\tau_{lm}} \cos(\omega_{lm} t + \gamma_{lm}), \qquad (1)$$

$$B_{lm} = \frac{\alpha_{lm} M}{D} \sqrt{(F_+ Y_+^{lm})^2 + (F_\times Y_\times^{lm})^2}, \qquad (2)$$

$$\gamma_{lm} = \phi_{lm} + m\beta + \arctan\left(\frac{F_\times Y_\times^{lm}}{F_+ Y_+^{lm}}\right), \qquad (3)$$

$$Y_{+,\times}^{lm}(\iota) = {}_{-2}Y_{lm}(\iota, \beta = 0) \pm (-1)^l {}_{-2}Y_{l-m}(\iota, \beta = 0), \qquad (4)$$

where α_{lm} and ϕ_{lm} are the mode amplitudes and phases, D is the luminosity distance to the source, ${}_{-2}Y_{lm}(\iota, \beta)$ are the spin-weighted spherical harmonics, and $F_{+,\times}(\theta, \phi, \psi)$ are the single-detector antenna patterns [44]. The angles ι and β describe the orientation of the BH, with ι (β) being the polar (azimuthal) angle of the wave propagation direction measured with respect to the BH spin axis. In the conventions of Refs. [45,46], the frequency-domain strain reads

$$\tilde{h}(f) = \sum_{l,m>0} B_{lm} \frac{-\omega_{lm} \sin\gamma_{lm} + (1/\tau_{lm} - i\omega)\cos\gamma_{lm}}{\omega_{lm}^2 - \omega^2 + 1/\tau_{lm}^2 - 2i\omega/\tau_{lm}}, \qquad (5)$$

where $f = \omega/2\pi$ is the GW frequency.

The dominant mode corresponds to $l = 2$, $m = 2$ (hereafter "22"), while the first subdominant is usually $l = 3$, $m = 3$ (hereafter "33"). Other modes might sometimes be stronger than the 33 mode for specific sources. For instance, the 33 mode is suppressed for $q \simeq 1$ or $\sin\iota \simeq 0$ (e.g., Refs. [33,47,48]). Here we perform a simple two-mode analysis considering the 22 and 33 modes only. Strictly speaking, the ringdown modes have angular distributions described by spheriodal, instead of spherical harmonics. However, for the final black-hole spins we consider, the 22 and 33 spin-weighted spherical harmonics have more than 99% overlap with the corresponding spin-weighted spheroidal harmonics [49,50], which is accurate enough for this study.[1] For simplicity, we restrict ourselves to nonspinning binary BHs with source-frame masses m_1 and m_2; we address the impact of this assumption in Sec. V. Redshifted masses $m_i(1 + z)$ are computed from the luminosity distance D using the Planck cosmology [51].

---

[1]We do note that, for the final black-hole spins we are considering, ${}_{-2}S_{22}$ and ${}_{-2}Y_{32}$ have overlap between 0.05 and 0.1, which does cause the 22 ringdown mode to show up significantly in the spherical-harmonic mode h_{32}. This is nevertheless consistent with the 99% overlap between ${}_{-2}Y_{22}$ and ${}_{-2}S_{22}$, because $\sum_{l'} |\langle {}_{-2}Y_{l'm} | {}_{-2}S_{lm} \rangle|^2 = 1$.

Mass M and spin j of the postmerger BH are estimated using fits to numerical relativity simulations [52,53] as implemented in Ref. [54]. Quasinormal frequencies ω_{lm} and decay times τ_{lm} are estimated from Ref. [29]. We estimate the excitation amplitudes α_{lm} given the mass ratio $q = m_2/m_1 \leq 1$ of the merging binary using the expressions reported by Ref. [43]. BH ringdown parameter estimation has been shown to depend very weakly on the phase offsets ϕ_{lm} [29], which we thus set to 0 for simplicity (cf. also Ref. [55]).

B. Waveform model and GR test

In BH spectroscopy, one assumes that quasinormal mode frequencies ω_{lm} and decay times τ_{lm} for different modes depend separately on M and j, and then look for consistencies between the different estimates.[2] Considering the 22 and 33 modes only, one can write the waveform as

$$h = h_{22}(M_{22}, j_{22}) + h_{33}(M_{33}, j_{33}) \qquad (6)$$

and use data to estimate the parameters:

$$\boldsymbol{\lambda} \equiv \{M_{22}, j_{22}, M_{33}, j_{33}\}. \qquad (7)$$

Deviations from GR may cause nonzero values of

$$\epsilon_M \equiv \frac{M_{22} - M_{33}}{(M_{22} + M_{33})/2}, \qquad \epsilon_j \equiv \frac{j_{22} - j_{33}}{(j_{22} + j_{33})/2}. \qquad (8)$$

We therefore seek to maximize our ability to estimate ϵ_M and ϵ_j from the observed data.

Given true values $\bar{\lambda}_i$, each independent noise realization will result in estimates $\tilde{\lambda}_i$ given by

$$\tilde{\lambda}_i = \bar{\lambda}_i + \delta\lambda_i, \qquad (9)$$

where $\delta\lambda_i$ are random variables driven by noise fluctuations in a way that depends on both the signal and the estimation scheme. Measured values of deviation from GR can be obtained by inserting measured values $\tilde{M}_{22,33}$ and $\tilde{j}_{22,33}$ into Eq. (8), resulting in

$$\tilde{\epsilon}_M = \frac{\tilde{M}_{22} - \tilde{M}_{33}}{(\tilde{M}_{22} + \tilde{M}_{33})/2}, \qquad \tilde{\epsilon}_j = \frac{\tilde{j}_{22} - \tilde{j}_{33}}{(\tilde{j}_{22} + \tilde{j}_{33})/2}. \qquad (10)$$

At linear order, one gets $\tilde{\epsilon}_M = \bar{\epsilon}_M + \delta\epsilon_M$ and $\tilde{\epsilon}_j = \bar{\epsilon}_j + \delta\epsilon_j$, with

$$\delta\epsilon_M = \frac{\bar{M}_{33}\delta M_{22} - \bar{M}_{22}\delta M_{33}}{(\bar{M}_{22} + \bar{M}_{33})^2/4}, \qquad \delta\epsilon_j = \frac{\bar{j}_{33}\delta j_{22} - \bar{j}_{22}\delta j_{33}}{(\bar{j}_{22} + \bar{j}_{33})^2/4}. \qquad (11)$$

In the absence of any deviations from GR, one has $\bar{M}_{22} = \bar{M}_{33} = \bar{M}$ and $\bar{j}_{22} = \bar{j}_{33} = \bar{j}$, but ϵ_M and ϵ_j will have statistical fluctuations given by

$$\delta\epsilon_M = \frac{\delta M_{22} - \delta M_{33}}{\bar{M}}, \qquad \delta\epsilon_j = \frac{\delta j_{22} - \delta j_{33}}{\bar{j}}. \qquad (12)$$

The levels of these fluctuations will quantify our ability to test GR. In fact, Eq. (12) is a good approximation to Eq. (11), as long as fractional deviation from GR is small, i.e., when $\bar{\epsilon}_M \ll 1$ and $\bar{\epsilon}_j \ll 1$.

C. Estimation errors

The covariance matrix σ_{ij}, namely, the expectation values

$$\sigma_{ij} \equiv \langle \delta\lambda_i \delta\lambda_j \rangle, \qquad (13)$$

can be bounded by the Fisher information formalism [56] (but see Ref. [57]). The conservative bound for the error is given by the inverse of the Fisher Information matrix:

$$\sigma_{ij} = \boldsymbol{\Gamma}_{ij}^{-1}, \boldsymbol{\Gamma}_{ij} = \left(\frac{\partial\tilde{h}}{\partial\lambda_i}\bigg|\frac{\partial\tilde{h}}{\partial\lambda_j}\right), \qquad (14)$$

where parentheses indicate the standard noise-weighted inner product.

In our case, the covariance matrix can be broken into blocks,

$$\boldsymbol{\Gamma}^{-1} = \begin{bmatrix} (\boldsymbol{\Gamma}^{-1})_{2222} & (\boldsymbol{\Gamma}^{-1})_{2233} \\ (\boldsymbol{\Gamma}^{-1})_{3322} & (\boldsymbol{\Gamma}^{-1})_{3333} \end{bmatrix}, \qquad (15)$$

corresponding to the couples (M_{22}, j_{22}) and (M_{33}, j_{33}). The diagonal block $(\boldsymbol{\Gamma}^{-1})_{2222}$ corresponds to errors when estimating (M_{22}, j_{22}) alone (marginalizing over other uncertainties), and the diagonal block $(\boldsymbol{\Gamma}^{-1})_{3333}$ corresponds to errors when estimating (M_{33}, j_{33}) alone (marginalizing over other uncertainties), while the nondiagonal blocks contain error correlations.

From the covariance matrix for $(M_{22}, j_{22}, M_{33}, j_{33})$, one obtains the following expectation values:

$$\langle \delta\epsilon_M^2 \rangle = \frac{\sigma_{M_{22}M_{22}} - 2\sigma_{M_{22}M_{33}} + \sigma_{M_{33}M_{33}}}{\bar{M}^2}, \qquad (16)$$

$$\langle \delta\epsilon_j^2 \rangle = \frac{\sigma_{j_{22}j_{22}} - 2\sigma_{j_{22}j_{33}} + \sigma_{j_{33}j_{33}}}{\bar{j}^2}, \qquad (17)$$

$$\langle \delta\epsilon_M \delta\epsilon_j \rangle = \frac{\sigma_{M_{22}j_{22}} - \sigma_{M_{33}j_{22}} - \sigma_{j_{22}M_{33}} + \sigma_{M_{33}j_{33}}}{\bar{M}\bar{j}}, \qquad (18)$$

which are elements of the covariance matrix of $(\delta\epsilon_M, \delta\epsilon_j)$. For concreteness, we define a scalar figure of merit,

---

[2]For simplicity, we only vary ω_{lm} and τ_{lm}, while keeping α_{lm} fixed to their GR values.

$$\delta \mathrm{GR} = \left| \begin{array}{cc} \langle \delta \epsilon_M^2 \rangle & \langle \delta \epsilon_M \delta \epsilon_j \rangle \\ \langle \delta \epsilon_M \delta \epsilon_j \rangle & \langle \delta \epsilon_j^2 \rangle \end{array} \right|^{1/4}, \qquad (19)$$

to quantify our ability to test GR. More specifically, $\delta \mathrm{GR}$ measures our statistical error in revealing deviations from GR. One has the strongest possible test of GR when $\delta \mathrm{GR} \to 0$, corresponding to $\mathbf{\Gamma}^{-1} \to \mathbf{0}$, in which case any deviation from GR will be revealed with vanishing statistical error. Large values of $\delta \mathrm{GR}$ would require larger deviations from GR [i.e., larger true values of (ϵ_M, ϵ_j)] in order to be detectable.

Given values of $\delta \mathrm{GR}$ from both a design and an optimized detector configuration, it is useful to define the narrow-band gain,

$$\zeta = \frac{\delta \mathrm{GR}^{(\mathrm{Design})} - \delta \mathrm{GR}^{(\mathrm{Optimized})}}{\delta \mathrm{GR}^{(\mathrm{Design})}}, \qquad (20)$$

where $\zeta = 1$ ($\zeta = 0$) means that the narrow banding procedure is maximally effective (irrelevant).

D. Error correlations between modes

We note that the 22–33 correlation components of the Fisher information matrix, as well as its inverse, are expected to be small, because the two modes are well separated in the frequency domain. In particular, $\partial h(\omega)/ \partial M_{22}$ and $\partial h(\omega)/\partial j_{22}$ peak near ω_{22} with widths $\sim 1/\tau_{22}$, while $\partial h(\omega)/\partial M_{33}$ and $\partial h(\omega)/\partial j_{33}$ peak near ω_{33} with widths $\sim 1/\tau_{33}$. For this reason, the pairs $(\delta M_{22}, \delta j_{22})$ and $(\delta M_{33}, \delta j_{33})$ are nearly statistically independent from each other. Estimation error for ϵ_M and ϵ_j can be viewed as (almost) independently contributed from the 22 and 33 modes and summed by quadrature. One has, approximately,

$$\langle \delta \epsilon_M^2 \rangle \approx \frac{\sigma_{M_{22} M_{22}} + \sigma_{M_{33} M_{33}}}{\bar{M}^2}, \qquad (21)$$

$$\langle \delta \epsilon_j^2 \rangle \approx \frac{\sigma_{j_{22} j_{22}} + \sigma_{j_{33} j_{33}}}{\bar{j}^2}, \qquad (22)$$

$$\langle \delta \epsilon_M \delta \epsilon_j \rangle \approx \frac{\sigma_{M_{22} j_{22}} + \sigma_{M_{33} j_{33}}}{\bar{M} \, \bar{j}}. \qquad (23)$$

In other words, the covariance matrix of $(\delta \epsilon_M, \delta \epsilon_j)$ is approximated by the sum of those of $(\delta M_{22}/\bar{M}, \delta j_{22}/\bar{j})$ and $(\delta M_{33}/\bar{M}, \delta j_{33}/\bar{j})$.

We quantify this claim by calculating values of $\delta \mathrm{GR}$ where the off-diagonal submatrices $(\mathbf{\Gamma}^{-1})_{3322}$ and $(\mathbf{\Gamma}^{-1})_{2233}$ are artificially set to zero. For the population of sources studied in Sec. IV B, and observed by LIGO, the median difference between the two estimates is as small as 1.6% (4.0%) for broadband (narrow-band) configurations.

For this reason, some insight can be gained by visualizing the error region in the (M_{22}, j_{22}) and (M_{33}, j_{33})

planes separately (cf. Sec. IV A): errors in $(\delta \epsilon_M, \delta \epsilon_j)$ are well approximated by the quadrature sum of errors indicated by those regions. We stress, however, that correlations are fully included in all values of $\delta \mathrm{GR}$ reported in the rest of this paper.

III. NARROW-BAND TUNINGS

As an example of a possible narrow-band setup, we consider the detuning of the signal-recycling cavity (cf. Refs. [18,20], where a similar setup was also explored). Second-generation GW detectors make use of signal-recycling optical configurations (or resonant side-band extraction) [58–60]. A signal-recycling mirror is placed at the dark port of a Fabry-Perot Michelson interferometer, which is the configuration used in first-generation detectors. The transmittance T_{SRM} of this mirror determines the fraction of signal light which is sent back into the arms, possibly with a detuning phase ϕ_{SRM}. Both these parameters affect the optical resonance properties of the interferometer [58,59], as well as its optomechanical dynamics [61,62]. Together with the homodyne readout phase ϕ_{hd}, T_{SRM} and ϕ_{SRM} are responsible for the quantum noise spectrum of the interferometer, allowing for noise suppression near optical and optomechanical resonances [63].

In this paper, we consider narrow banding of both LIGO in its design configuration and future third-generation detectors. The LIGO design noise curve is a finalized experimental setup which allows us to perform a focused assessment of the impact of narrow banding onto BH spectroscopy over a large number of sources. However, more sensitive ground-based interferometers are currently being planned and are expected to be operational by the 2030s [39,64]. Multiband observations and LISA forewarnings might happen with a network of ground-based detectors perhaps 10 times more sensitive than LIGO.

In order to select the best detuned configuration to perform BH spectroscopy, one needs to choose values of $(T_{\mathrm{SRM}}, \phi_{\mathrm{SRM}}, \phi_{\mathrm{hd}})$ that boost sensitivity around the 33 frequency. For LIGO, we generate 60^3 noise curves with equal spacing in $\phi_{\mathrm{SRM}} \in [-0.12\pi, 0.12\pi]$, $T_{\mathrm{SRM}} \in [0.001, 0.2]$, and $\phi_{\mathrm{hd}} \in [0, \pi]$. This parameter space is capable of capturing the central frequencies of both the 22 and 33 mode for binaries with $q \in [0.2$–$0.9]$ and total masses $m_1 + m_2 \in [20 \, M_\odot$–$100 \, M_\odot]$. Noise curves are generated using pyGWINC [65]. The LIGO design configuration corresponds to $T_{\mathrm{SRM}} = 0.2$, $\phi_{\mathrm{SRM}} = 0$, and $\phi_{\mathrm{hd}} = \pi/2$. The broadband noise curves reported by Refs. [38,66] are reproduced within $\Delta \log S_n / \log S_n \lesssim 0.2\%$ throughout the entire frequency band. For each given source, we select the optimal noise curve that minimizes $\delta \mathrm{GR}$ among those we precomputed. Figure 1 illustrates this procedure for an optimally oriented source similar to GW150914 [67]. This narrow-band setting corresponds to a noise curve with $\phi_{\mathrm{SRM}} \simeq 0.21$, $T_{\mathrm{SRM}} \simeq 0.02$, and $\phi_{\mathrm{hd}} \simeq 2.24$.

While the design of third-generation detectors is still being discussed, it is anticipated that squeezed-vacuum injection will be used. Squeezer and cavity properties need to be optimized together to determine the optimal configuration. Fully tackling this interplay is outside the scope of this paper. We have nonetheless attempted one such study, where *both* the filter cavity for the squeezed vacuum [68,69] and the signal-recycling cavity of the Cosmic Explorer [39] design have been optimized to target the ringdown emission of GW150914 (cf. Fig. 1).

IV. RESULTS

A. Boosting subdominant modes

Confidence ellipses [70] constructed from $(\mathbf{\Gamma}^{-1})_{2222}$ and $(\mathbf{\Gamma}^{-1})_{3333}$ are shown in Fig. 2 for sources similar to GW150914. In the left panel, we consider the narrow banding of a LIGO detector for a source similar to GW150914 at the optimistic distance of $D = 40$ Mpc. This value is consistent with the closest GW source detected so far [71] and corresponds to $\sim 1/10$ of the actual distance of GW150914. In the right panel, we consider the detuning of a third-generation detector (Cosmic Explorer) for the case of the same source at $D = 400$ Mpc.

The behavior of the ellipses of Fig. 2 illustrates the main point of our analysis. In the standard broadband configuration, the 22 mode is observed very well, thus resulting in a small confidence region. At the same time, the 33 mode is observed poorly, resulting in a large ellipse. As in the case of current events [72], this is roughly equivalent to a single measurement of M and j based on the 22 mode only, rather than a test of the theory. Narrow-band tunings boost the detectability of the 33 mode, while marginally reducing that of the dominant 22 excitation. Consequently, the two confidence ellipses are more similar to each other, resulting in a more powerful constraint of the Kerr metric.

For a source like GW150914 at 40 Mpc, narrowband tunings in LIGO boost prospects to perform BH spectroscopy from δGR $= 0.056$ to δGR $= 0.032$, thus offering the opportunity to improve constraints on the BH no-hair theorems by $\zeta = 43\%$. The same source at $D = 400$ Mpc observed by a third-generation detector will present a higher gain of $\zeta = 59\%$. Rescaling D between the left and right panels of Fig. 2 allows us to asses the potential of optimization in future interferometers. In particular, ellipses in the right panel are smaller than those in the left panel because, while the distance was changed from 40 to 400 Mpc, the expected improvement in the sensitivity of Cosmic Explorer is more than a factor of 10 compared to LIGO. We obtain a larger gain ζ for third-generation detectors, because quantum noise is expected to dominate more over classical sources of noise compared to current interferometers [39]. There is, therefore, more room to take advantage of modifications in optical configurations.
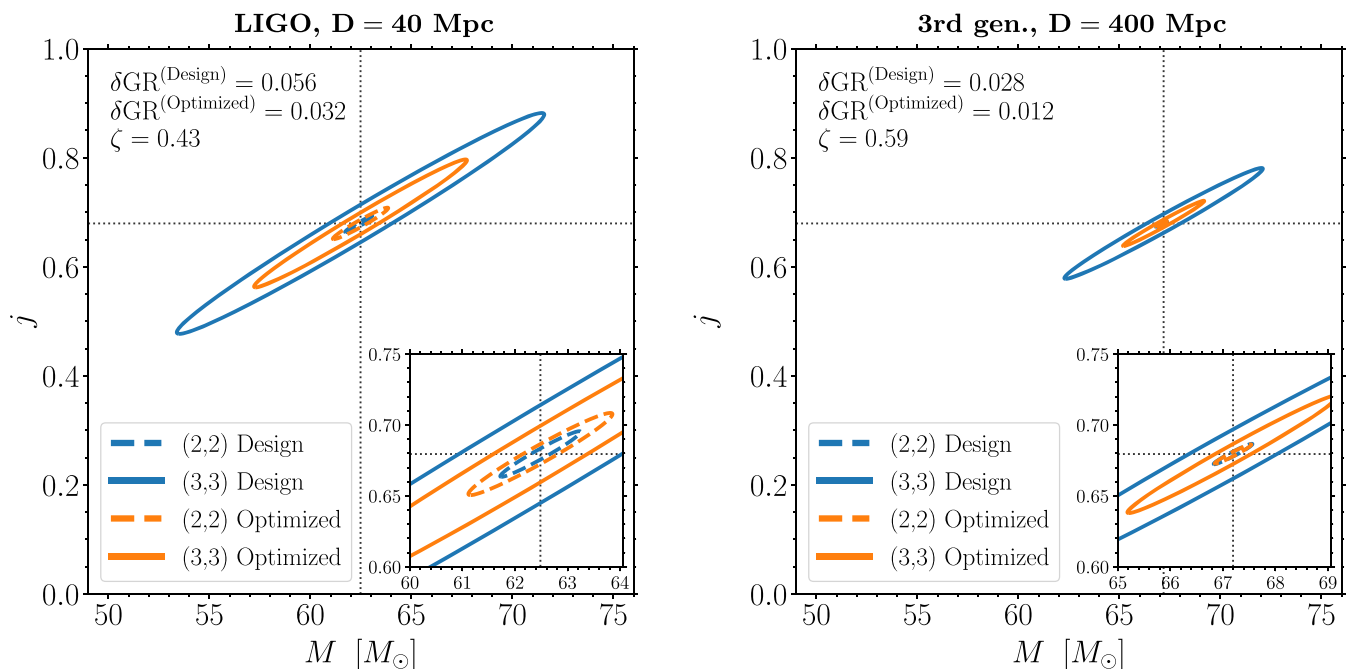
FIG. 2. 1σ confidence ellipses for the 22 (dashed) and 33 (solid) modes observed by GW detectors in their designed (blue) and optimized narrow-band configurations (orange). In both panels, the source is a perturbed Kerr BH of mass $M = 62.5\ M_\odot$ and spin $j = 0.68$ (dotted lines), resulting from the merger of a GW150914-like system ($m_1 + m_2 = 65\ M_\odot$, $q = 0.8$, $\iota = 150°$, $\beta = 0$) assuming optimal orientation ($\theta = \phi = \psi = 0$). The left panel assumes an optimistic luminosity distance $D = 40$ Mpc and the LIGO detector in its design sensitivity. The right panel is generated assuming a third-generation detector optimized for the same system and a realistic luminosity distance $D = 400$ Mpc.
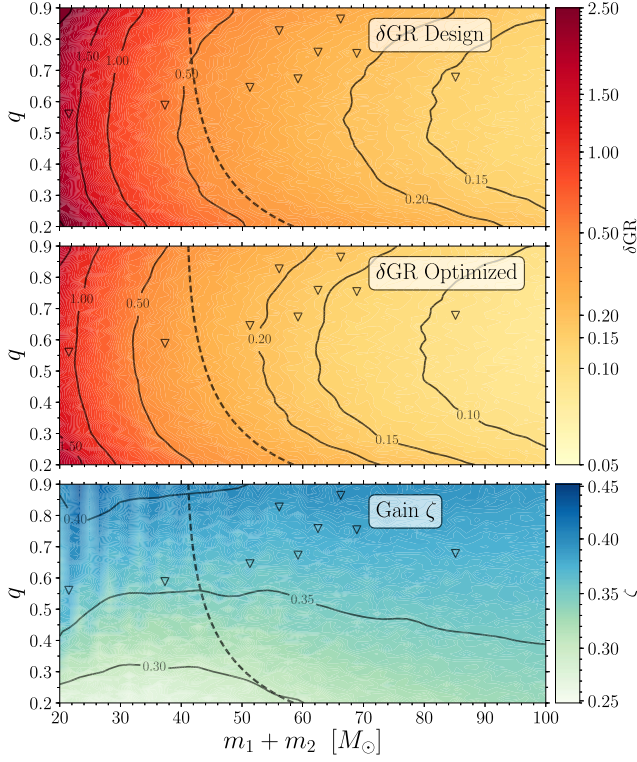
FIG. 3. Top and middle panels show median values of δGR for LIGO at design sensitivity and with narrow-band tuning, respectively; bottom panel shows the median gain ζ. Data are shown as a function of total mass $m_1 + m_2$ and mass ratio q of the merging binaries; medians are computed over $\theta, \iota, \beta, \phi$, and ψ. The distance is fixed to $D = 100$ Mpc. Binaries to the right of the dashed lines have sky-averaged LISA SNRs greater than 8 (these are computed following Ref. [3] using the updated noise curve of Ref. [37] and the nominal mission duration $T_{obs} = 4$ yr; the initial frequency is estimated such that the binary merges in T_{obs}). Triangles indicate measured LIGO events (we show the medians of the posterior distributions from Ref. [1]).

B. Population study

We now assess the impact of this procedure as a function of the source properties. We generate a population of sources drawing $\cos\theta$ and $\cos\iota$ uniformly in $[-1, 1]$, and drawing β, ϕ, and ψ uniformly in $[-\pi, \pi]$, with fixed[3] distance $D = 100$ Mpc. Figure 3 shows the median values of δGR as a function of the masses of the merging BHs. The top panel assumes LIGO in its design configuration, and the middle panel presents results optimizing the narrow-band setup individually for each source, while the gain ζ is shown in the bottom panel.

A few interesting trends are present. First, the best systems to perform BH spectroscopy (i.e., low values of

---

[3] Since δGR is directly proportional to D, results in Fig. 3 can be rescaled to different distances. Cosmological effects might push the ringdown frequencies of some high-mass events out of band, thus somewhat decreasing the gain.

δGR) have intermediate mass ratio $0.3 \lesssim q \lesssim 0.7$. Both ringdown amplitudes α_{22} and α_{33} are suppressed for $q \to 0$, while $\alpha_{22} \gg \alpha_{33}$ for $q \to 1$. Second, tests of GR are weaker (higher δGR) for lower-mass systems. These binaries have f_{33} close to the edge of the sensitivity window of the interferometer, thus making mode distinguishability harder. The LISA SNR also increases with the total mass and the mass ratio. In particular, binaries with $m_1 + m_2 \lesssim 40\ M_\odot$ are not likely to be associated with confirmed forewarnings (cf. Ref. [10]).

A key point of our findings is illustrated in the gain values ζ reported in the bottom panel of Fig. 3. From Eq. (20), ζ quantifies the potential improvement in BH spectroscopy achievable with narrow-band tunings. Median gains are larger than 25% over the entire parameter space, and individual sources can reach values up to 50%. In particular, higher gains are achieved for large-q systems. This agrees with the expectation that both modes are suppressed at $q \to 0$, while only the 33 mode is suppressed at $q \to 1$. Narrow-band tunings shift the detector sensitivity closer to f_{33} at the expense of the 22 mode, and are thus more effective if its excitation is large such that the resulting sensitivity loss can be more easily absorbed.

V. DISCUSSION

The possibility of optimizing ground-based operation assumes that LISA observations of the early inspiral accurately predict the ringdown frequencies (in particular f_{33}), thus providing information on *how* ground-based interferometers should be optimized. We estimate LISA errors on f_{33} as follows. For a given source with chirp mass M_c and symmetric mass ratio η, we first estimate f_{33} assuming zero spins (this is our working assumption used above). Inspired by the results reported in Fig. 3 of Ref. [3] (computed as in Ref. [73]), we model LISA errors as log-normal distributions centered at $\Delta M_c/M_c = 10^{-6}$, $\Delta\eta/\eta = 6 \times 10^{-3}$ with widths $\sigma = 0.5$. We then calculate f_{33} for a new binary with masses $M_c + \Delta M_c$ and $\eta + \Delta\eta$, and spins with magnitudes uniform in $[0, 1]$ and isotropic directions. In practice, we are assuming that LISA will not provide any information on the spins. This is a conservative, but realistic, assumption because spins enter at high post-Newtonian order and are going to be very challenging to detect at low frequencies [74]. This procedure is iterated over a population of sources with masses uniformly distributed in $[10, 100]\ M_\odot$. The median of the errors Δf_{33} is 11 Hz, while the 90th percentile is 46 Hz. For the case of cavity detuning explored here, typical bandwidths are $\gtrsim 200$ Hz (cf. Fig. 1), sensibly larger than the predicted errors. Therefore, we estimate that the risk of *missing* the source because the detector was detuned in the wrong configuration is very limited. The precision with which LISA will estimate the time of coalescence is at most of $\mathcal{O}(100\ \text{s})$ [3] and should not pose significant challenges in the planning strategy. Moreover, only some of the ground-based instruments of the

network could be optimized, while the rest are maintained in their broadband configuration.

Cavity detuning presents significant experimental challenges, regarding both detector characterization and lock acquisition, and might ultimately turn out to be impractical (see Ref. [75] for an exploration of these issues on the LIGO 40 m prototype). We note that narrow banding can also be achieved without detuning by using, e.g., twin-recycling [76] or speed-meter [77] configurations; such a possibility is currently being studied to optimize for postmerger signals from neutron-star mergers for future detectors [19]. Beyond targeted narrow banding around the 33 frequency, optimization can also be achieved by reconfiguring future ground-based interferometers in different ways. For the planned third-generation detector Cosmic Explorer [39], the quantum noise is expected to dominate all other noise sources by more than a factor of 2 for frequencies $\gtrsim 40$ Hz with a chosen bandwidth of 800 Hz. With forewarnings, a less broadband configuration (even without detuning) could be chosen to significantly improve BH spectroscopy. In the case of the Einstein Telescope [64], a broad bandwidth is achieved by a xylophone that contains two different interferometers optimized for different frequency ranges. It is conceivable that a strong LISA forewarning might prompt a reconfiguration of the two interferometers to optimize for BH spectroscopy.

Space-based GW observatories like LISA will surely provide exquisite tests of GR with supermassive BH observations [29]. As shown here, they can further be exploited to improve BH spectroscopy in the different regime of lower-mass, higher-curvature BHs observed by LIGO and future ground-based facilities. More generally, forewarnings from space-based detectors will provide the opportunity to configure ground-based instruments to their most favorable configuration to perform targeted measurements and improve their science return.

---

[1] B. P. Abbott *et al.* (LIGO and Virgo Scientific Collaborations), arXiv:1811.12907.

[2] P. Amaro-Seoane *et al.* (LISA Core Team), arXiv:1702 .00786.

[3] A. Sesana, Phys. Rev. Lett. **116,** 231102 (2016).

[4] A. Nishizawa, E. Berti, A. Klein, and A. Sesana, Phys. Rev. D **94,** 064020 (2016).

[5] K. Breivik, C. L. Rodriguez, S. L. Larson, V. Kalogera, and F. A. Rasio, Astrophys. J. Lett. **830,** L18 (2016).

[6] A. Nishizawa, A. Sesana, E. Berti, and A. Klein, Mon. Not. R. Astron. Soc. **465,** 4375 (2017).

[7] X. Chen and P. Amaro-Seoane, Astrophys. J. Lett. **842,** L2 (2017).

[8] K. Inayoshi, N. Tamanini, C. Caprini, and Z. Haiman, Phys. Rev. D **96,** 063014 (2017).

[9] J. Samsing, D. J. D'Orazio, A. Askar, and M. Giersz, arXiv: 1802.08654.

[10] D. Gerosa, S. Ma, K. W. K. Wong, E. Berti, R. O'Shaughnessy, Y. Chen, and K. Belczynski, Phys. Rev. D **99,** 103004 (2019).

[11] E. Barausse, N. Yunes, and K. Chamberlain, Phys. Rev. Lett. **116,** 241104 (2016).

[12] S. Vitale, Phys. Rev. Lett. **117,** 051102 (2016).

[13] K. W. K. Wong, E. D. Kovetz, C. Cutler, and E. Berti, Phys. Rev. Lett. **121,** 251102 (2018).

[14] K. Kyutoku and N. Seto, Phys. Rev. D **95,** 083525 (2017).

[15] W. Del Pozzo, A. Sesana, and A. Klein, Mon. Not. R. Astron. Soc. **475,** 3485 (2018).

[16] R. X. Adhikari, Rev. Mod. Phys. **86,** 121 (2014).

[17] S. A. Hughes, Phys. Rev. D **66,** 102001 (2002).

[18] H. Miao, H. Yang, and D. Martynov, Phys. Rev. D **98,** 044044 (2018).

[19] D. Martynov, H. Miao, H. Yang, F. Hernandez Vivanco, E. Thrane, R. Smith, P. Lasky, W. E. East, R. Adhikari,

A. Bauswein, A. Brooks, Y. Chen, T. Corbitt, T. Corbitt, H. Grote, Y. Levin, C. Zhao, and A. Vecchio, arXiv: 1901.03885.

[20] D. Tao and N. Christensen, Classical Quantum Gravity **35,** 125002 (2018).

[21] C. V. Vishveshwara, Nature (London) **227,** 936 (1970).

[22] E. Berti, V. Cardoso, and A. O. Starinets, Classical Quantum Gravity **26,** 163001 (2009).

[23] R. P. Kerr, Phys. Rev. Lett. **11,** 237 (1963).

[24] W. Israel, Commun. Math. Phys. **8,** 245 (1968).

[25] B. Carter, Phys. Rev. Lett. **26,** 331 (1971).

[26] M. Heusler, *Black Hole Uniqueness Theorems* (Cambridge University Press, Cambridge, England, 1996).

[27] S. Detweiler, Astrophys. J. **239,** 292 (1980).

[28] O. Dreyer, B. Kelly, B. Krishnan, L. S. Finn, D. Garrison, and R. Lopez-Aleman, Classical Quantum Gravity **21,** 787 (2004).

[29] E. Berti, V. Cardoso, and C. M. Will, Phys. Rev. D **73,** 064030 (2006).

[30] E. Berti, K. Yagi, H. Yang, and N. Yunes, Gen. Relativ. Gravit. **50,** 49 (2018).

[31] E. Berti, A. Sesana, E. Barausse, V. Cardoso, and K. Belczynski, Phys. Rev. Lett. **117,** 101102 (2016).

[32] A. Maselli, K. D. Kokkotas, and P. Laguna, Phys. Rev. D **95,** 104026 (2017).

[33] V. Baibhav, E. Berti, V. Cardoso, and G. Khanna, Phys. Rev. D **97,** 044048 (2018).

[34] H. Yang, K. Yagi, J. Blackman, L. Lehner, V. Paschalidis, F. Pretorius, and N. Yunes, Phys. Rev. Lett. **118,** 161101 (2017).

[35] S. Bhagwat, M. Okounkova, S. W. Ballmer, D. A. Brown, M. Giesler, M. A. Scheel, and S. A. Teukolsky, Phys. Rev. D **97,** 104065 (2018).

[36] R. Brito, A. Buonanno, and V. Raymond, Phys. Rev. D **98,** 084038 (2018).

[37] N. Cornish and T. Robson, Classical Quantum Gravity **36,** 105011 (2019).

[38] B. P. Abbott *et al.* (LIGO and Virgo Scientific Collaborations), Living Rev. Relativity **19,** 1 (2016).

[39] B. P. Abbott *et al.* (LIGO and Virgo Scientific Collaborations), Classical Quantum Gravity **34,** 044001 (2017).

[40] S. Khan, S. Husa, M. Hannam, F. Ohme, M. Pürrer, X. J. Forteza, and A. Bohé, Phys. Rev. D **93,** 044007 (2016).

[41] S. A. Teukolsky, Astrophys. J. **185,** 635 (1973).

[42] E. Berti, J. Cardoso, V. Cardoso, and M. Cavaglià, Phys. Rev. D **76,** 104044 (2007).

[43] I. Kamaretsos, M. Hannam, S. Husa, and B. S. Sathyaprakash, Phys. Rev. D **85,** 024018 (2012).

[44] K. S. Thorne, in *Three Hundred Years of Gravitation* (Cambridge University Press, Cambridge, England, 1987), pp. 330–458.

[45] F. Echeverria, Phys. Rev. D **40,** 3194 (1989).

[46] L. S. Finn, Phys. Rev. D **46,** 5236 (1992).

[47] L. London, D. Shoemaker, and J. Healy, Phys. Rev. D **90,** 124032 (2014); **94,** 069902(E) (2016).

[48] S. Bhagwat, D. A. Brown, and S. W. Ballmer, Phys. Rev. D **94,** 084024 (2016).

[49] E. Berti and A. Klein, Phys. Rev. D **90,** 064012 (2014).

[50] M. Giesler, M. Isi, M. Scheel, and S. Teukolsky, arXiv: 1903.08284.

[51] P. A. R. Ade *et al.* (Planck Collaboration), Astron. Astrophys. **594,** A13 (2016).

[52] E. Barausse, V. Morozova, and L. Rezzolla, Astrophys. J. **758,** 63 (2012).

[53] E. Barausse and L. Rezzolla, Astrophys. J. Lett. **704,** L40 (2009).

[54] D. Gerosa and M. Kesden, Phys. Rev. D **93,** 124066 (2016).

[55] J. G. Baker, W. D. Boggs, J. Centrella, B. J. Kelly, S. T. McWilliams, and J. R. van Meter, Phys. Rev. D **78,** 044046 (2008).

[56] C. Cutler and É. E. Flanagan, Phys. Rev. D **49,** 2658 (1994).

[57] C. L. Rodriguez, B. Farr, W. M. Farr, and I. Mandel, Phys. Rev. D **88,** 084013 (2013).

[58] B. J. Meers, Phys. Rev. D **38,** 2317 (1988).

[59] G. Heinzel, J. Mizuno, R. Schilling, W. Winkler, A. Rüdiger, and K. Danzmann, Phys. Lett. A **217,** 305 (1996).

[60] G. Vajente, in *Advanced Interferometers and the Search for Gravitational Waves* (Springer, New York, 2014), Vol. 404, p. 57.

[61] A. Buonanno and Y. Chen, Phys. Rev. D **65,** 042001 (2002).

[62] A. Buonanno and Y. Chen, Phys. Rev. D **67,** 062002 (2003).

[63] A. Buonanno and Y. Chen, Phys. Rev. D **64,** 042006 (2001).

[64] M. Punturo *et al.*, Classical Quantum Gravity **27,** 194002 (2010).

[65] P. Fritschel, D. Coyne *et al.*, dcc.ligo.org/T010075, git.ligo.org/gwinc/pygwinc.

[66] D. Shoemaker *et al.*, dcc.ligo.org/LIGO-T0900288.

[67] B. P. Abbott *et al.* (LIGO and Virgo Scientific Collaborations), Phys. Rev. Lett. **116,** 061102 (2016).

[68] J. Harms, Y. Chen, S. Chelkowski, A. Franzen, H. Vahlbruch, K. Danzmann, and R. Schnabel, Phys. Rev. D **68,** 042001 (2003).

[69] A. Buonanno and Y. Chen, Phys. Rev. D **69,** 102004 (2004).

[70] D. Coe, arXiv:0906.4123.

[71] B. P. Abbott *et al.* (LIGO and Virgo Scientific Collaborations), Phys. Rev. Lett. **119,** 161101 (2017).

[72] B. P. Abbott *et al.* (LIGO and Virgo Scientific Collaborations), Phys. Rev. Lett. **116,** 221101 (2016).

[73] E. Berti, A. Buonanno, and C. M. Will, Phys. Rev. D **71,** 084025 (2005).

[74] A. Mangiagli, A. Klein, A. Sesana, E. Barausse, and M. Colpi, Phys. Rev. D **99,** 064056 (2019).

[75] R. L. Ward, Ph.D. thesis, Caltech, 2010.

[76] A. Thüring, C. Gräf, H. Vahlbruch, M. Mehmet, K. Danzmann, and R. Schnabel, Opt. Lett. **34,** 824 (2009).

[77] P. Purdue and Y. Chen, Phys. Rev. D **66,** 122004 (2002).